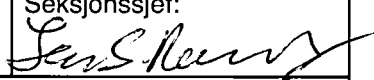


Rapport nr. 90.160		ISSN 0800-3416		Åpen/Ettersøkt	
<b>Tittel:</b> Detailed geophysical investigations of the Stuoragurra postglacial fault, Finnmark, northern Norway					
<b>Forfatter:</b> O. Olesen, H. Henkel, O.B. Lile, E. Mauring, J.S. Rønning			<b>Oppdragsgiver:</b> NGU		
<b>Fylke:</b> Finnmark			<b>Kommune:</b> Kautokeino		
<b>Kartbladnavn (M. 1:250 000)</b> Nordreisa			<b>Kartbladnr. og -navn (M. 1:50 000)</b> 1933 IV Masi		
<b>Forekomstens navn og koordinater:</b> Fidnajakka 597700-7687500			<b>Sidetall:</b> 35		<b>Pris:</b> kr. 95,-
<b>Feltarbeid utført:</b> 1988-1990		<b>Rapportdato:</b> 18.03.1991		<b>Prosjektnr.:</b> 61.1886.47	
<b>Seksjonssjef:</b> 					
<b>Sammendrag:</b> The postglacial Stuoragurra Fault (SF) lies within the Mierujav'ri-Sværholt Fault Zone which is situated in the extensive Proterozoic terrain of Finnmark, northern Norway. It is a southeasterly dipping reverse fault and can be traced fairly continuously for 80 km from Skarrejav'ri south of Masi to Lævnjasjåkka northeast of Iesjav'ri. Detailed geophysical investigations and drilling have been carried out in the Fidnajakka area 10 km to the south of Masi. The geology of the area is dominated by quartzites. A c. 1 m thick layer of fault gouge detected in the drillholes is thought to represent the actual fault surface.  Resistivity measurements reveal low-resistivity zones in the hanging-wall block as well as in the foot-wall block of the SF. These low-resistivity zones lie within a several hundred metre wide belt and are interpreted to be due to fracturing of the quartzites along the regional Mierujav'ri-Sværholt Fault Zone. Within the Fidnajakka area, however, the resistivity of the hanging-wall block of the SF is typically lower than in the foot-wall, indicating more intense fracturing in the hanging-wall. Vertical electrical soundings show a low-resistivity layer at depth in the eastern hanging-wall block, which corroborates other evidence that the fault dips to the southeast.  Within the survey area, there exist two possibilities for the course of the postglacial reverse fault at depth: (a) The fault is listric with a dip of 50° in the uppermost 10 m of the subsurface and a dip of 30° at a depth between 25 and 40 m. (b) The fault continues at depth from the surface with a dip of 50-60°. If model (a) is correct, the SF will be represented by a 1 m thick gouge which occurs in a drillhole and the fault will be parallel with the foliation at depth.  When interpreting the refraction seismic data precautions had to be taken as one tended to interpret greater depths to bedrock than those found from percussion drilling. This phenomenon is probably caused by fractured and weathered bedrock occurring in a "hidden layer" with intermediate velocity to the above-lying overburden and the under-lying 'fresh' bedrock but occurring in a layer which is too thin to be recognised in the time-distance plot. Detailed topographical data proved very useful for estimating the dip of the fault zone in the upper part of the subsurface. Additional data from georadar measurements could be used to map the thickness of the overburden and, when combined with the digital topography, these measurements could be used to map the topography of the bedrock surface. Highly reflective bedrock on the georadar diagrams is interpreted to be fractured and weathered quartzite and single reflectors can be interpreted as fault zones.					
Emneord Geofysikk		Elektromagnetisk måling		Kvartsitt	
Berggrunnsgeologi		Elektrisk måling		Kvartær	
Forkastning		Seismikk		Fagrapport	

## CONTENTS

1 INTRODUCTION .....	4
2 GEOLOGICAL SETTING .....	4
3 METHODS .....	5
3.1 Digital topography .....	5
3.2 Georadar .....	6
3.3 Electrical measurements .....	6
3.4 Electromagnetics .....	7
3.5 Seismics .....	8
4 RESULTS .....	8
4.1 Digital topography .....	8
4.2 Georadar .....	9
4.3 Resistivity measurements .....	9
4.4 Refraction seismics .....	10
4.5 Percussion drilling .....	12
5 DISCUSSION .....	12
6 CONCLUSIONS .....	13
7 ACKNOWLEDGEMENTS .....	14
8 REFERENCES .....	14
LIST OF FIGURES .....	18

Odleiv Olesen, Herbert Henkel\*, Ole Bernt Lile\*\*, Eirik Muring & Jan Steinar Rønning Norges geologiske undersøkelse, P.O.Box 3006, N-7002 TRONDHEIM, \*Sveriges geologiska undersökning, P.O.Box 670, S-751 28 UPPSALA, \*\* Universitetet i Trondheim , NTH, N-7034 TRONDHEIM-NTH

## 1 INTRODUCTION

Our view of the stability of Norwegian bedrock has changed significantly in recent years. Direct stress measurements and interpretation of seismic activity have shown us that Fennoscandia is under NW-SE compression (Zoback et al. 1989, Bungum et al. in press). There is growing evidence that this stress, mostly related to the plate tectonic 'ridge push' force, is causing faulting along old zones of weakness in northern Fennoscandia.

The Stuoragurra Fault, SF, is manifested in the surface as a fault scarp and was discovered in 1983 during follow-up work of geophysical interpretations within the Finnmark Programme and has been reported by Olesen (1984, 1988) and Muir Wood (1989). Similar fault scarps (Fig. 1), interpreted to be post- or late-glacial, occur in adjacent parts of Finland (Kujansuu 1964), Sweden (Lagerbäck 1979), USSR (Tanner 1930) and in Troms, northern Norway (Grønlie 1922, Tolgensbakk & Sollid 1988). At Skipskjølen on Varangerhalvøya similar escarpments can be observed on aerial photographs within the Trollfjord-Komagelv Fault Zone. Since the glacial overburden is missing, it is not possible to date this fault. It is, however, indicated in Fig. 1 as a potential Late Quaternary postglacial fault because of its similarity in appearance to the SF. Roberts (in press) has reported a 5.8 cm offset of a drillhole during 3 years in a road-cut in Laksefjord, Finnmark.

When estimating hazard with respect to the disposal of radioactive waste and the construction of large installations such as offshore platforms, petroleum pipelines and hydropower plants it is essential to know the neotectonics of the actual area. An improved understanding of the neotectonics in Finnmark may also throw light on the development of the passive continental margin in the Norwegian Sea and the Barents Sea. The SF is easily accessible by roads in the Masi area. Detailed geophysical investigations have therefore been carried out to map the SF in detail, with special attention to the extent of the fault at depth. At an introductory stage, two areas located north of Masi and west of Fidnajakka (Fig. 2) were selected for a reconnaissance study with electrical and electromagnetic methods. It is important to note that the geology of the Masi area is dominated by mafic and intermediate metavolcanic rocks and micaschists whereas the Fidnajakka area is dominated by quartzites. EM-anomalies in the area north of Masi were mainly found to reflect sulphides and graphite in the volcanosedimentary rocks whereas in the Fidnajakka area they reflect faults. Further detailed studies, including georadar, electromagnetic and seismic methods, were therefore carried out in the Fidnajakka area to map the fault itself.

## 2 GEOLOGICAL SETTING

The postglacial Stuoragurra Fault, SF, runs parallel to the northwestern margin of the Jer'gul Gneiss Complex and is situated within the Mierjav'ri-Sværholt Fault Zone, MSFZ. Postglacial faulting occurs most commonly either along the margins of duplex structures or within them (Olesen et al. 1990b), but northeast of Iesjav'ri such faulting occurs within the main fault zone. It is mainly situated within the quartzites of the Masi Formation. The SF can be traced fairly continuously over a distance of 80 km,

from Skarrejav'ri south of Masi in a northeasterly direction to Lævnjasjåkka northeast of Iesjav'ri (Fig. 2). There is, however, a 20 km break in this line to the southwest of Iesjav'ri. The southern part of the SF is shown on the 1:50,000 scale geological map, 1933 IV Masi, by Solli (1988). The faults occur as marked, linear and sharp steps in the generally smoothed till cover (Fig. 3). The downthrown side lies to the northwest with a maximum observed vertical displacement of seven metres.

The SF transects glaciofluvial deposits northeast of Iesjav'ri (Olesen 1988) and an esker northeast of Masi (Fig. 4) and, as such, certain sections of the zone at least must have been formed after the deglaciation estimated to 9,000 BP (Olsen in prep.). Four kilometres to the southwest of Masi (UTM coord. 601800 - 7703650), 0.5 - 1.0 m deep, rounded hollows occur in a glaciofluvial deposit. One of them has a 0.5 m high rim of silt around the central depression. These structures may represent disturbances in waterlain sediments (Lagerbäck 1990) induced by seismicity during the formation of the SF. Locally one metre wide and one metre deep cracks parallel to the escarpment can be observed in the hanging wall-block of the SF (Fig. 5). These are interpreted to be accommodation faults (R. Gabrielsen pers. comm. 1990) which were formed during reverse faulting.

North of Masi the SF cuts amphibolites and an albite diabase within the Suoluvuobmi Formation. Brecciation is observed at all locations where the bedrock is exposed in the fault escarpment (Fig. 6) and is also observed along the entire length of the MSFZ on Finnmarksvidda. Hence, brittle deformation is consequently believed to have occurred during the formation of the MSFZ and not during the formation of the younger SF. Within the survey area the quartzite is folded, with fold axes parallel to the MSFZ. Alternating thin and thick limbs of the folds dip 20° to the southeast and almost vertically, respectively (C. Talbot pers. comm. 1988). An axial plane foliation dips at approximately 30° to the southeast. This geological information is included in the final interpretation (Fig. 16).

### 3 METHODS

#### 3.1 Digital topography

The topographic map of the area was constructed by Fjellanger Widerøe (A. Lorvik pers. comm.) using a photogrammetric method, with contours of 2 metres at a scale of 1:2,000. The northernmost part of the map is shown in Fig. 8. Isolines have been digitised and this data-set was then interpolated to a square grid of 5x5 m using the minimum curvature method (Briggs 1974, Swain 1976). In addition, a 3D perspective model (Fig. 7) of this grid was constructed using the ERDAS image processing system (Erdas 1990). A transect or 'fish net' plot over a subset of the data-set was also constructed using the SURFER software package by Golden Software Inc. (1989). This 3D surface model was used as a base for the interpretation of the ground-geophysical data (Fig. 16).

If the uppermost part of the postglacial fault is assumed to be a planar surface, the intersection line between the fault and the surface can be used to construct the dip of the fault applying the stratum contour method. The fault scarps in the Fidsnájåkka area appear to bend as a response to differences in topographic relief.

### 3.2 Georadar

The system employed for georadar measurements was a Subsurface Interface Radar, SIR-7, manufactured by Geophysical Survey Systems Inc. (GSSI). The central frequency of the antenna is 80 MHz, with a depth of penetration of approximately 20 m (Fig. 10).

The system is of impulse radar type and provides a continuous profile of subsurface conditions. An electromagnetic pulse is generated at the surface, with reflections from the surface and the subsurface interfaces being displayed on a continuous strip-chart recorder. Travel times for the reflected pulses can be converted to the depths to various interfaces if the velocity of propagation is known.

The effective propagation velocity of the pulse through the earth is derived from the equation:

$$v = \frac{2D}{t} \quad (3.1)$$

where D in the present study is the depth to bedrock, determined from drilling, and t is the elapsed time between the transmitted and received pulse from the bedrock surface.

The effective relative dielectric constant,  $\epsilon$ , of the subsurface material is determined from the equation

$$\epsilon = \frac{c^2}{v^2} \quad (3.2)$$

where c is the propagation velocity in free space ( $3 \times 10^8$  m/s). The georadar diagrams from Profiles 805-807 are presented in Fig. 9. Note that the vertical scale is greater than the horizontal. The locations of the profiles are shown in Fig. 8 and the reflectors interpreted from the georadar diagrams are illustrated in Fig. 10. The terrain along the profiles has been surveyed and the line drawings of the reflectors are adjusted according to the levelled topography.

### 3.3 Electrical measurements

Electrical profiling as well as vertical electrical sounding were undertaken to map the low-resistivity zones representing the brecciated and weathered part of the quartzite.

The DC-resistivity profiling data in Fig. 11 and induced polarisation (IP) data were acquired with the NGU-produced IP4 instrument (Dalsegg & Brandhaug 1990) using a gradient array. A potential electrode spacing of 10 m and a current electrode spacing of 660 m were used, with the penetration of the DC-resistivity data estimated to be 100-200 m. This method yields the apparent resistivity perpendicular to the fault.

The ABEM Terrameter SAS300 with a Schlumberger electrode configuration (Telford et al. 1976) was

used for the vertical electrical sounding. The apparent resistivity measurements were interpreted using the VESABS computer-programme developed by Kihle (1978). The programme assumes that the ground consists of parallel layers of differing thickness and resistivity. The response of the model is calculated and the model is adjusted until an optimal fit between the theoretical and measured curves is attained. Information from boreholes and georadar can be used to fix the thickness of the uppermost layers. The model, however, is still ambiguous because of two factors: 1. The equivalence principle states that thickness and resistivity of a layer can vary between certain limits, but have virtually the same response: 2. Suppression occurs when the resistivity of a layer is intermittent between those of the layers above and below. If the thickness of this layer is low it will not manifest itself on the sounding curve.

Another complicating factor is that the assumption of parallel layers in the interpretation programme may not be met within heterogeneous bedrock.

### 3.4 Electromagnetics

In regions of high resistivity, electromagnetic methods can be used to detect large water-containing fracture zones in the bedrock (Henkel & Eriksson 1980, Eriksson 1980, Henkel 1988). In-situ resistivity measurements using the VLF and Slingram methods provide information about the soil and the bedrock conductivity. Such measurements allow more detailed studies of the location and width of fault zones because they can discriminate between brecciated and normal crystalline rocks with differing resistivity. Eriksson (1980) and Henkel (1988, in press) have documented how the resistivity of crystalline bedrock is dependent on fracturing:

<u>degree of fracturing</u>	<u>resistivity, ohmm</u>
non fractured bedrock	25 000
fractured bedrock	2 000 - 6 000
strongly fractured bedrock	600
<u>fault gouge</u>	<u>30</u>

The following EM instruments were used along Profile 807 (Fig. 8): the VLF EM-16R instrument by Geonics (1972) using the GYD station with a frequency of 19.0 kHz, and the Geonics (1980) EM-31 slingram with a frequency of 9.8 KHz and a coil spacing of 3.66 m.

In order to determine the electrical resistivity of the ground, the VLF 16R measures the ratio and the phase angle between the horizontal electric and magnetic fields of the wave propagated by distant VLF (very low frequency) radio transmitters. The penetration depth of the EM 16R instrument is 160 and 230 m when the resistivity of the bedrock is 2000 and 4000 ohmm, respectively and the applied frequency is 20 KHz (Geonics 1972). Non-isotropic resistivity conditions within the penetration depth result in a shift of the phase angle. Depending on the value of the phase angle,  $\phi$ , three different cases of resistivity distributions may occur: 1)  $\phi < 45^\circ$  - the resistivity increases downwards; 2)  $\phi = 45^\circ$  - isotropic resistivity distribution within the penetration depth; 3)  $\phi > 45^\circ$  - the resistivity decreases downwards. When assuming a horizontal two-layer model, nomograms by Geonics (1972) can be used to estimate depth to the lowermost layer and the resistivity of this layer when the resistivity of the

uppermost layer is known. Only flat-lying and gently dipping fault zones can, however, be interpreted with this model. The VLF method yields the resistivity parallel to the direction to the transmitter (Hjelt et al. 1985) and cannot be directly compared to the data acquired from the DC-resistivity profiling if there is significant anisotropy. The VLF resistivity measurements were carried out with 20 m station spacing along Profile 807.

A magnetic dipole transmitter in the EM-31 instrument induces very small currents in the earth. A weak secondary magnetic field originating from these currents is, under certain conditions, linearly related to the ground conductivity. The effective depth of investigation is 6 m (Geonics 1980).

An additional slingram instrument provided by the Swedish Geological Company, with a 40 m coil spacing and a 18 KHz signal, were also tested along Profile 807. This slingram method did not, however, provide any additional information.

### 3.5 Seismics

The seismic refraction method was used to determine depth to the bedrock and to locate the postglacial fault within the bedrock. Refraction seismics also gave information about the occurrence of fractured and weathered bedrock. The geophone spacing was 5 m except for the four geophones adjacent to the shot points where the spacing was 2.5 m. The measurements were performed using an ABEM TRIO 12 channel analog seismograph.

In addition to the refraction seismic method, reflection seismics were tested in the area using the common offset technique. The test, however, was not successful. The reason for this is thought to be the loss of acoustic energy in the dry sand where the source (shot-gun) was located.

## 4 RESULTS

### 4.1 Digital topography

The postglacial fault cuts through a N-S trending ridge within the framed survey area in Fig. 7. Assuming the fault to be a plane, the stratum contour method can be used to calculate the dip of the fault. It was found to be  $50^\circ$  in the uppermost 10 m of the ground. This is consistent with the interpretation of the percussion drilling data, indicating that the fault is listric.

In its southernmost section, the SF cuts across a slope and a plane in the terrain (Fig. 7). Application of the stratum contour method in this area gives a dip of c.  $35^\circ$ . The height difference between the foot of the slope and the plane is 30 m.

From the course of the SF in the topography the main sense of movement along the SF must be reverse. The existence of a minor strike-slip component, however, cannot be ruled out. A dextral component

of movement could explain the presence a small lake along the SF in the centre of Fig. 7 as a sag pond (Slemmons & Depolo 1986), but the evidence for this is not compelling. We think that this lake is caused mainly by damming by the reverse fault. This depression may, however, also have formed during glacial erosion prior to the formation of the SF.

## 4.2 Georadar

Georadar sections taken along Profiles 805-810 are presented in Fig. 9 with the interpretations shown in Fig. 10. In the interpretations, reflectors are adjusted according to the topography, and coordinate 0 on all profiles is situated on the crest of the postglacial fault escarpment. On most of the georadar profiles the bedrock surface appears as a distinct reflector. Using the depths from drillholes 4 and 5 (Figs. 8 & 15) and the elapsed times from the georadar diagrams (Fig. 9), the propagation velocity in the glaciofluvial sand is estimated to 0.09 and 0.10 m/ns, respectively, using equation 3.1 given above. Applying an average velocity of 0.095 m/ns yields a dielectric constant of 10 (from equation 3.2 in the previous section). This corresponds to the upper limit of previously published estimates, 5-10, for natural dry sand in Sweden and Denmark (Berg et al. 1983) and therefore was considered reliable enough to reduce the remaining data. Continuous reflectors within the glaciofluvial deposit are thought to represent layering of material with differing grain sizes. Highly reflective areas within the bedrock, indicated with cross-hatching in Fig. 10, are situated to the west of the escarpment on the profiles. These areas are thought to be highly brecciated and weathered bedrock. This interpretation is confirmed by percussion drilling (DH 2 & 3 in Figs. 8 & 10). The N-S trending ridge in Figs. 7 & 8 has a core of bedrock which is exposed along the postglacial fault in Profile 806.

## 4.3 Resistivity measurements

When interpreting the apparent resistivity profiling curves in Fig. 11, the differing depth of penetration achieved by the various systems employed must be taken into account. The EM 31 slingram maps the resistivity of the overburden since the depth of resolution is 6 metres while the DC and VLF apparent resistivity methods map the resistivity of the overburden and bedrock down to approximately 200 m. The apparent resistivity curves along Profile 807 in Fig. 11 show that the eastern (hanging-wall) block generally has a lower resistivity than the western one. The DC-resistivity shows 1000 - 2000 ohmm in the hanging-wall block compared with 4000 - 20,000 ohmm in the foot-wall block. This indicates a more fractured bedrock in the hanging-wall which is supported by the VLF resistivity measurements. The low phase angles (<45°) to the east of 50 m in Fig. 11 show that the resistivity increases at depth beneath the hanging-wall block. Using the nomograms by (Geonics 1972) along section 50-100 m west on Profile 807 assuming a resistivity of 1000 ohmm for the hanging-wall block indicates a resistivity larger than 3000 ohmm of the foot-wall block and a depth of approximately 70 m. The high phase angles (>45°) to the west of 10 m show that the resistivity within the foot-wall decreases with depth, supporting the interpretation of another fault-zone out-cropping at approximately -100 m (see below). A decrease of the apparent DC-resistivity can also be observed at coordinate -100 m.

Vertical electrical sounding data (Figs. 12 & 13) also show a complex fracturing of the bedrock with



low-resistivity zones in the hanging-wall block as well as in the foot-wall block. Vertical electrical soundings (Fig. 12) show the lowest resistivity layer at some depth in the eastern block, consistent with the observation of eastward-dipping faults. The vertical electrical soundings (Fig. 12) to the west of the postglacial fault indicate low-resistivity layers at depth, interpreted as zones of fractured bedrock in the diagrams in Figs. 13 & 16. These zones can be traced on the topographical map and approaches the postglacial fault to the south (Fig. 8). To the south of the small lake in the centre of Fig. 7, the SF steps approximately 30 m to the right to follow the westernmost fault zone.

The resistivity measurements consequently indicate that the SF is situated within a more than two hundred metre wide fault zone which we interpret to be part of the regional Mierujav'ri-Sværholt Fault Zone (Olesen et al. 1990a,b). We cannot, however, totally rule out the possibility that the low resistivity, locally, is partly caused by the presence of sulphides. Approximately 30 m to the west of the escarpment on Profile 805 (Fig. 8) there is a spring of water causing a 25 m long and 3-5 m wide zone where there is no vegetation other than the flower *Viscaria alpina* and some moss. This is caused by naturally copper-contaminated groundwater emerging from the westernmost interpreted fault zone in Fig. 8. Chemical analyses of three soil samples from this zone show copper contents of 0.36, 0.50 and 1.34 %. Induced polarisation (Telford et al. 1976) measurements along Profile 807 show, however, that the IP effect is 1-2 %, which demonstrates that the content of the sulphides along this profile is very low and therefore cannot explain the observed low-resistivity zones.

#### 4.4 Refraction seismics

The interpreted velocities of the quartzites within the survey area are 2400-4100 m/s, which are low compared with published data on fresh quartzites: 4500-6200 m/s (Carmichael 1989), 4500-5100 m/s (Atlas Copco ABEM 1987) and 5800 m/s (Reich 1943). Intercalations of 'fresh' albite diabase within the quartzite would have an even higher velocity. We interpret the low velocities to be caused by a generally high incidence of fracturing and faulting of the bedrock within the survey area. Similar low-velocity zones have earlier been reported to coincide with postglacial faults in the Lansjärv area in northern Sweden (Henkel 1988). The width of the zone in the Fidnajakka area is greater than in the Lansjärv area, indicating a higher degree of fracturing in the vicinity of the SF compared with the Lansjärv Fault.

The results from the refraction seismic profiles are therefore generally in agreement with those of the other methods - with the exception of one major discrepancy: the intersection by the drillhole of the bedrock surface is 5 m shallower than the depth obtained from the refraction seismic (Fig. 14). From the percussion drilling we know that the groundwater surface is located in the bedrock at a depth of 35 m along the drillhole. No water-saturated sediments with increased velocity therefore exist. The reason for the observed phenomenon is thus believed to be a highly shattered and fractured bedrock in the hanging-wall block. A similar discrepancy between refraction seismics and fault scarp excavations in the hanging-wall block has been reported from the Lansjärv Fault (Lagerbäck 1990), and is also associated with decreased velocity in a layer of shattered and fractured bedrock between the overburden and more competent bedrock. Even if this velocity is higher than that of the overburden it may still not be recognised as a distinct event if the layer is too thin. Such a layer is called the 'blind-zone' (Hawkins & Maggs 1961) or the 'hidden layer' (Lund 1974, Telford et al. 1976).

The maximum thickness of this layer may be calculated from the equation

$$t_2 = k_2 \frac{t_h}{1 + ck_2} \quad (4.1)$$

on the assumption that the overburden has a minimum thickness

$$t_1 = \frac{t_h}{1 + ck_2} \quad (4.2)$$

where  $t_h$  is the estimated depth from the two-layer model and  $c$  and  $k_2$  are two velocity-dependent factors:

$$c = \frac{v_1}{v_2} \cdot \frac{\sqrt{v_3^2 - v_2^2}}{\sqrt{v_3^2 - v_1^2}} \quad (4.3)$$

$$k_2 = \frac{1}{\sqrt{v_3^2 - v_2^2}} \left[ \frac{V_3 \sqrt{V_2^2 - V_1^2} - V_2 \sqrt{V_2^2 - V_1^2}}{V_2 - V_1} + \frac{V_3 \sqrt{V_2^2 - V_1^2} - V_2 \sqrt{V_3^2 - V_1^2}}{V_1} \right] \quad (4.4)$$

where  $v_1$ ,  $v_2$  and  $v_3$  are the velocities of the overburden, 'hidden zone' and fresh bedrock, respectively.

When applying the velocities 800 m/s and 3800 m/s (Fig. 14) for overburden and 'fresh' bedrock, respectively, in addition to the known thickness of overburden in drillholes nos. 4 and 5, we can calculate the maximum thickness of the hidden layer. On the assumption that the velocity of this zone is 1300 - 1500 m/s, the maximum thickness is 11 and 8 m, respectively. If the velocity of the hidden layer is greater than 1300 - 1500 m/s, the maximum thickness must be smaller.

In boreholes nos. 4 and 5 (Fig. 15) the well log indicates a thickness of 29 m and 11 m, respectively, of brecciated bedrock in the uppermost part of the hanging-wall block. These estimates are considerably larger than the calculated maximum thickness of a possible hidden layer, especially for borehole no. 5. The thickness of the brecciated bedrock is, however, based on visual judgements of the drilling speed and this parameter cannot directly be related to the seismic velocity. We observe from the drill cuttings in Fig. 15 that the content of fine-grained material is higher in the uppermost part of drillhole 4, indicating a more fractured and possibly weathered rock. We therefore infer that the discrepancy between the depths obtained from the refraction seismics and from the percussion drilling is most likely caused by highly shattered and fractured bedrock in the upper part of the hanging-wall block. A generally intense brittle deformation of the hanging-wall block of the SF is also indicated by a 1 m wide accommodation fault which is situated 40 m from the SF scarp to the north of Masi (Fig. 5).

#### 4.5 Percussion drilling

Two shallow drillholes and two deeper drillholes are located within the survey area (Fig. 8). Drillholes nos. 2 and 3 are located in the foot-wall block on Profile 806, immediately to the west of the escarpment, while nos. 4 and 5 are situated along Profile 807 in the hanging-wall block, 60 m and 30 m to the east of the escarpment, respectively. The depths of the four drillholes were 13.5, 7.5, 61 and 31 m, respectively, and the bedrock surface was encountered at the depths of 4.5, 5.5, 12.0, and 7.3 m. Samples of the drill chips from the bedrock are shown in Fig. 15. Fault gouge of approximately 1 m thickness at depths of 37.5 m and 25.5 m in drillholes 4 and 5 is interpreted to represent the postglacial fault at depth. This implies a dip of the postglacial fault of ca. 30° to the southeast. At shallower depths the fault plane must dip more steeply, perhaps up to 50° (Profile 807 in Fig. 10), in order for it to outcrop in the escarpment.

#### 5 DISCUSSION

The geophysical methods that we applied were capable of detecting the differing properties of the hanging-wall and foot-wall blocks in the SF. Information on overburden thickness and bedrock topography was also acquired from the measurements. However, none of the tested geophysical methods was able to detect the postglacial fault itself.

A dip estimate of 50° in the upper 10 m of the ground can be inferred from the topographical data. Because of the collapse of the scarp and subsequent erosion we consider that the error in this estimate can be about 10°. From the percussion drilling, a dip of 30° can be interpreted from the intersection with a 1 m thick fault gouge at depths of 37 m and 25 m in drillholes 4 and 5 (Figs. 10 & 16). This would indicate that the fault has a listric shape. An approximately 1 m thick zone of similar fault gouge (R. Gabrielsen, pers. comm. 1990) representing a postglacial fault is exposed in a road-cut in Yrkje, Southwest Norway (Anundsen & Gabrielsen 1990).

Faulting may not be listric, however, if the drilled fault gouge does not really represent the postglacial fault. This would imply that drillholes nos. 4 and 5 were abandoned prematurely. If the fault is steeper than 55°, it would not have been penetrated by either of the two drillholes. To find out if the Stuuragurra Fault represents a listric fault or not we recommend core-drilling a 200 m deep hole at an angle of 60° from a location 50 m to the southeast of the scarp at Profile 807.

We have managed to integrate the results from this detailed survey with the interpretation of aeromagnetic data (Olesen et al. 1990b) which shows that the SF in the Fidnajakka area is situated within a 1.4 km wide complex zone in which there are four 50-100 m wide albite diabases. The dip of these diabases within the present survey area is 40-50° to the southeast which is consistent with the dip of the fault zones. The margin of one of these diabases is encountered in drillhole no. 4 (Figs. 10 & 16).

About 3 km to the northeast, the SF is situated along the contact of an albite diabase. The SF then gradually turns to a more northerly trend into the Biggevarri Duplex (Olesen et al. 1990b). The albite diabases continue in the same NNE direction along the southeastern border of this duplex

and gradually become steeper (Olesen et al. 1990b). This group of 1815±24 Ma old albite diabases (Krill et al. 1985) can be traced almost continuously for 75 km in a northeasterly direction to Iesjav'ri and has intruded along the regional Mierujav'ri-Sværholt Fault Zone (Olesen et al. 1990a,b).

## 6 CONCLUSIONS

1. Based on the information currently available, within the survey area there are two possibilities for the change in the course of the postglacial reverse fault with depth: (a) The fault is listric with a dip of c. 50° in the uppermost 10 m of the subsurface and a dip of c. 30° at a depth between 25 and 40 m; (b) The fault continues at depth from the surface with a dip of 50-60°. If model (a) is correct, the SF will be represented by a 1 m thick gouge and the fault will be parallel with the foliation at depth. If model (b) is correct, the drillholes in the hanging-wall block were abandoned prematurely and did not penetrate the fault. When combining the different geophysical results and geological features we find model (a) to be the more likely solution.
2. The resistivity measurements show complex fracturing of the bedrock with low-resistivity zones in the hanging-wall block as well as in the foot-wall. The SF is thus interpreted to be situated within a several hundred metre wide fault zone. This zone is part of the Biggevarri Duplex within the regional Mierujav'ri-Sværholt Fault Zone.
3. Generally, within the Fidnajákka area, it can be stated that the resistivity of the hanging-wall block of the SF is low, indicating a more fractured bedrock than in the foot-wall block.
4. The main sense of movement along the SF is reverse. The existence of a minor strike-slip component, however, cannot be ruled out.
5. When interpreting the refraction seismic data, precautions had to be taken since depth tended to be overestimated. This phenomenon is most likely caused by fractured and weathered bedrock occurring in a 'hidden layer' with intermediate velocity to the above-lying overburden and the under-lying 'fresh' bedrock but occurring in a layer which is too thin to be recognised on the time-distance plot.
6. Detailed topographical data proved very useful for estimating the dip of the fault zones close to the surface.
7. Measurements of the physical properties, seismic velocity and electrical resistivity, along the SF indicate the location of faulted and fractured bedrock but do not display any detailed three-dimensional image of the complex faulting.
8. Georadar measurements were used to map the thickness of the overburden and, combined with the digital topography, could be used to map the topography of the bedrock surface. Highly reflective bedrock is interpreted as fractured and weathered quartzite and single reflectors can be interpreted as fault zones.

## 7 ACKNOWLEDGEMENTS

This work was partially financed by the Royal Norwegian Council for Scientific and Industrial Research (Grant 13220 to Odleiv Olesen), the Geological Survey of Norway and the Norwegian Institute of Technology, University of Trondheim. Norsk teknisk byggekontroll a/s, NOTEBY, kindly provided the georadar equipment for this survey. David Roberts, Jan Sverre Sandstad, Arne Solli and Professors Roy Gabrielsen and Christopher Talbot have contributed with valuable advice and discussions. To all these persons and institutions we express our sincere thanks. We are also indebted to Drs. Peter Walker and David Roberts for critically reading the manuscript and for suggestions towards its improvement. We are further grateful to Randi Blomsøy, Gunnar Grønli and Torbjørn Haugen for preparing the figures.

## 8 REFERENCES

- Anundsen, K. & Gabrielsen, R.H. 1990: Neotectonics, Sunnhordland Region. Guide to excursion, Tectonics and Structural Geology Studies Group, October 5th 1990. Unpubl. Structural Geology Group, University of Bergen Report 5, 29 pp.
- Atlas Copco ABEM 1987: ABEM instruction manual, ABEM Terraloc Mk II seismic system, Printed Matter No. 93047. Atlas Copco ABEM, Bromma, Sweden, 185 pp.
- Berg, F., Andreasen, F. & Ahrentzen, P. 1983: Georadar til sand- og gruskortlægning. Et samarbejdsprojekt mellem fredningsstyrelsen, Danmarks Geologiske Undersøgelse og Statens Vejlaboratorium. Statens Vejlaboratorium Internal Report 147, 44 pp.
- Briggs, I.C. 1974: Machine contouring using minimum curvature. *Geophysics* 39, 39-48.
- Bungum, H., Alsaker, A., Kvamme, L.B. & Hansen, R.A. in press: Seismicity and seismotectonics of Norway and nearby continental shelf areas. *J. Geophys. Res.*
- Carmichael, R.S. 1989: Practical handbook of physical properties of rocks and minerals. CRC Press, Inc., Boca Raton, Florida, 741 pp.
- Dalsegg, E. & Brandhaug, K. 1990: Beskrivelse av IP. NGU Internal Report 90.001, 52 pp.
- Erdas 1990: 3D module, version 7.4.1, August 1990. ERDAS Inc., Atlanta, USA. 12 pp.
- Eriksson, L. 1980: Elektriska och magnetiska metoder för påvisande av svaghetszoner i berg (Abstract in English). Geophysical Report, Sveriges geologiska undersökning, SGU, 8012, 17 pp.

- Geonics 1972: Operating manual for EM16R direct reading ground resistivity meter (attachment to EM16 VLF EM). Geonics Ltd., Toronto, Canada. 23 pp.
- Geonics 1980: Operating manual for EM31 non-contacting terrain conductivity meter. Geonics Ltd., Toronto, Canada. 56 pp.
- Golden Software, Inc. 1989: Surfer, version 4, Reference manual. Golden, Colorado, 354 pp.
- Grønlie, O.T. 1922: Strandlinjer, moræner og skjælføremster i den sydlige del av Troms fylke. *Nor. geol. unders.* 94, 39 pp.
- Hawkins, L.V., & Maggs, D. 1961: Nomograms for determining maximum errors and limiting conditions in seismic refraction survey with a blind-zone problem. *Geophysical Prospecting* 9, 526-532.
- Henkel, H. 1988: Tectonic studies in the Lansjärv region. Svensk kärnbränslehantering AB Technical Report 88-07, 66 pp.
- Henkel, H. in press: Geophysical aspects of meteorite impact craters in eroded shield environments with emphasis on electrical resistivity measurements. *Tectonophysics*
- Henkel, H. & Eriksson, L. 1980: Interpretation of low altitude airborne magnetic and VLF measurements for identification of fracture zones. In: M. Bergman (ed.) *Subsurface Space*. Pergamon Press, Oxford.
- Henkel, H., Hult, K., Eriksson, L. & Johansson, L. 1983: Neotectonics in northern Sweden - geophysical investigations. Svensk kärnbränsleförsörjning AB/Avdelning KBS, Technical Report 83-57, 64 pp.
- Hjelt, S.E., Kaikkonen, P. & Pietilä, R. 1985: On the interpretation of VLF resistivity measurements. *Geoexploration* 23, 171-181.
- Kihle, O. 1978: VESABS - et program for interaktiv tolkning av vertikale elektriske sonderinger. NGU programme documentation 78-02, 8 pp.
- Krill, A.G., Berg, S., Lindahl, I., Mearns, E.W., Often, O. and Olerud, S., Olesen, O., Sandstad, J.S., Siedlecka, A., Solli, A. 1985: Rb-Sr, U-Pb, and Sm-Nd isotopic dates from the Precambrian rocks of Finnmark, *Nor. geol. unders. Bull.* 403, 37-54.
- Kujansuu, R. 1964: Nuorista sirroksista Lapissa. Summary: Recent faults in Lapland. *Geologi* 16, 30-36.
- Lagerbäck, R. 1979: Neotectonic structures in northern Sweden. *Geologiska Föreningens i Stockholm Förhandlingar* 100 (1978), 271-278.
- Lagerbäck, R. 1990: Late Quaternary faulting and paleoseismicity in northern Fennoscandia, with

- particular reference to the Lansjärv area, northern Sweden. *Geologiska Föreningens i Stockholm Förhandlingar* 112, 333-354.
- Lund, C.E. 1974: The hidden layer in seismic prospecting. *Geologiska Föreningens i Stockholm Förhandlingar* 96, 199-203.
- Muir Wood, R. 1989: Extraordinary deglaciation reverse faulting in northern Fennoscandia. In: S. Gregersen & P.W. Basham (eds.) *Earthquakes at North-Atlantic passive margins: neotectonics and postglacial rebound*. NATO ASI series. Series C, Mathematical and physical sciences, vol. 266. Kluwer Academic Publishers, Dordrecht, The Netherlands, 141-173.
- Olesen, O. 1988: The Stuoragurra Fault, evidence of neotectonics in the Precambrian of Finnmark, northern Norway. *Nor. Geol. Tidsskr.* 68, 107-118.
- Olesen, O. 1984: Sen-/post-glaciale forkastninger ved Masi, Finnmark. NGU Report 84.171, 27 pp.
- Olesen, O., Roberts, D., Henkel, H., Lile, O.B. & Torsvik, T. H. 1990a: Aeromagnetic and gravimetric interpretation of regional structural features in the Caledonides of West Finnmark and North Troms, northern Norway. *Nor. geol. unders. Bull.* 419, 1-24.
- Olesen, O., Henkel, H. & Lile, O.B. 1990b: Major fault zones within the Proterozoic Kautokeino Greenstone Belt, Finnmark, Norway: combined interpretation of geophysical data. NGU Report 90.161. 32 pp.
- Olsen, L. in prep.: KARASJOK. Quaternary geological map, scale 1:250,000 with description. Abstract in English. Geological Survey of Norway.
- Reich, H. 1943: *Taschenbuch der angewandten geophysik*. Akademische Verlagsgesellschaft, Leipzig, 407 pp.
- Roberts, D. 1991: A contemporary small-scale thrust-fault from near Lebesbye, Finnmark. *Norsk Geol. Tidsskr.*, (in press).
- Siedlecka, A. 1985: Geology of the Iesjav'ri - Skoganvarre area, Northern Finnmarksvidda, North Norway. *Norges geologiske undersøkelse* 403, 103-112.
- Slemmons, D.B. & Depolo, C.M. 1986: Evaluation of active faulting and associated hazards. In R.E. Wallace (ed.) *Active tectonics*. National Academy Press, Washington, D.C., 45-62
- Solli, A. 1988: MASI 1933 IV - berggrunnsgeologisk kart - M 1:50 000. *Norges geologiske undersøkelse*.
- Swain, C.J. 1976: A Fortran IV program for interpolating irregularly spaced data using the difference equations for minimum curvature. *Computers & Geosciences* 1, 231-240.

Tanner, V. 1930: Studier över kvartärsystemet i Fennoskandias nordliga delar IV. Bulletin de la Commission Géologique de Finlande 88, 594 pp.

Telford, W.M., Geldart, L.P., Sheriff, R.E. & Keys, D.A. 1976: Applied geophysics. Cambridge University Press, Cambridge. 860 pp.

Tolgensbakk, J. & Sollid, J.L. 1988: Kåfjord, kvartærgeologi og geomorfologi 1:50 000, 1634 II. Geografisk institutt, Universitetet i Oslo.

Zoback, M.L. & 28 co-authors 1989: Global patterns of tectonic stress. Nature 341, 291-298.



## LIST OF FIGURES

Fig. 1. Late Quaternary faults in northern Fennoscandia compiled from Grønlie (1922), Tanner (1930), Kujansuu (1964), Lagerbäck (1979,1988) and Tolgensbakk & Sollid (1988). The area covering the Stuoragurra Fault (Fig. 2) is framed.

Fig. 2. Postglacial faults on Finnmarksvidda. MSFZ - Mierujav'ri-Sværholt Fault Zone.

Fig. 3. Oblique aerial photograph of the Stuoragurra Fault (UTM 610200 - 7716200) looking east, approximately 10 km to the NNE of Masi. The location is shown in Fig. 2.

Fig. 4. The SF (in the middle of the picture) cutting through an esker 12 km NNE of Masi (UTM 611400 - 7717300); looking SW. The location is shown in Fig. 2.

Fig. 5. A 30 m long, 1 m wide and 1 m deep trench parallel to the escarpment in the hanging-wall block of the SF (UTM 604600 - 7710400). The distance from the slightly curved trench to the escarpment is 40 m. The location is shown in Fig. 2.

Fig. 6. Polished breccia of quartzite from Fidnajákka (UTM 596700 - 7687500). Mineral grains are crushed along fractures. The main secondary mineral present is chlorite. The location is shown in Fig. 2.

Fig. 7. 3D terrain model from the Fidnajákka area. The vertical scale is exaggerated by a factor of 3. The survey area (Fig. 16) is indicated by the frame.

Fig. 8. Detailed topographical map from the Fidnajákka area. The survey area (Fig. 16) is indicated by the frame.

Fig. 9. Georadar diagrams. Coordinate 0 on all the profiles is situated on the crest of the postglacial fault escarpment.

Fig. 10. Interpretation of georadar diagrams. Coordinate 0 on all the profiles is situated on the crest of the postglacial fault escarpment. In Profile 807, data from percussion drilling is added to the georadar interpretation below the penetration limit.

Fig. 11. Apparent resistivity measurements along Profile 807. The direction to the transmitter GYD (19 KHz) which is used for the VLF 16R measurements, is to the SW which is almost parallel to the postglacial fault

Fig. 12. Vertical electrical sounding along Profile 807.

Fig. 13. Interpretation of vertical electrical sounding along Profile 807.

Fig. 14. A) Refraction seismics along Profile 807. B) Profiles intersecting Profile 807 at 80E and 80W, respectively.

Fig. 15. Photograph of drill chips from the percussion drilling.

Fig. 16. Interpretation synthesis of model A (listric fault) for the SF as a block diagram, looking south. Note that Profile 807 in this diagram is a mirror image of the geophysical profiles along Profile 807 in Figs. 9-14 and that coordinate 85 in the present figure coincides with coordinate 0 in Figs. 9-14.

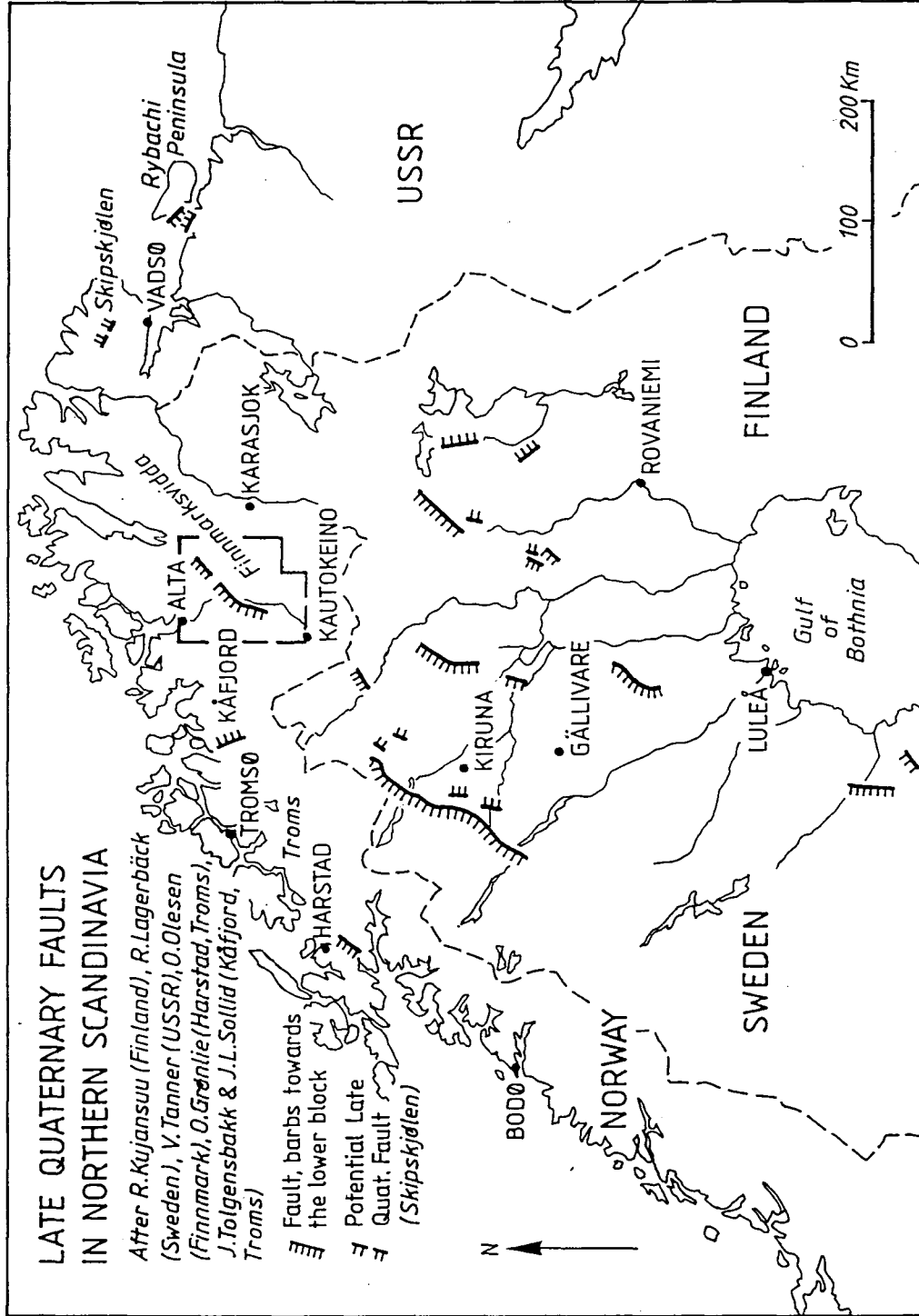


Fig. 1. Late Quaternary faults in northern Fennoscandia compiled from Grønlie (1922), Tanner (1930), Kujansuu (1964), Lagerbäck (1979, 1988), Olesen (1988) and Tolgensbakk & Sollid (1988). The area covering the Stuoragurra Fault (Fig. 2) is framed.

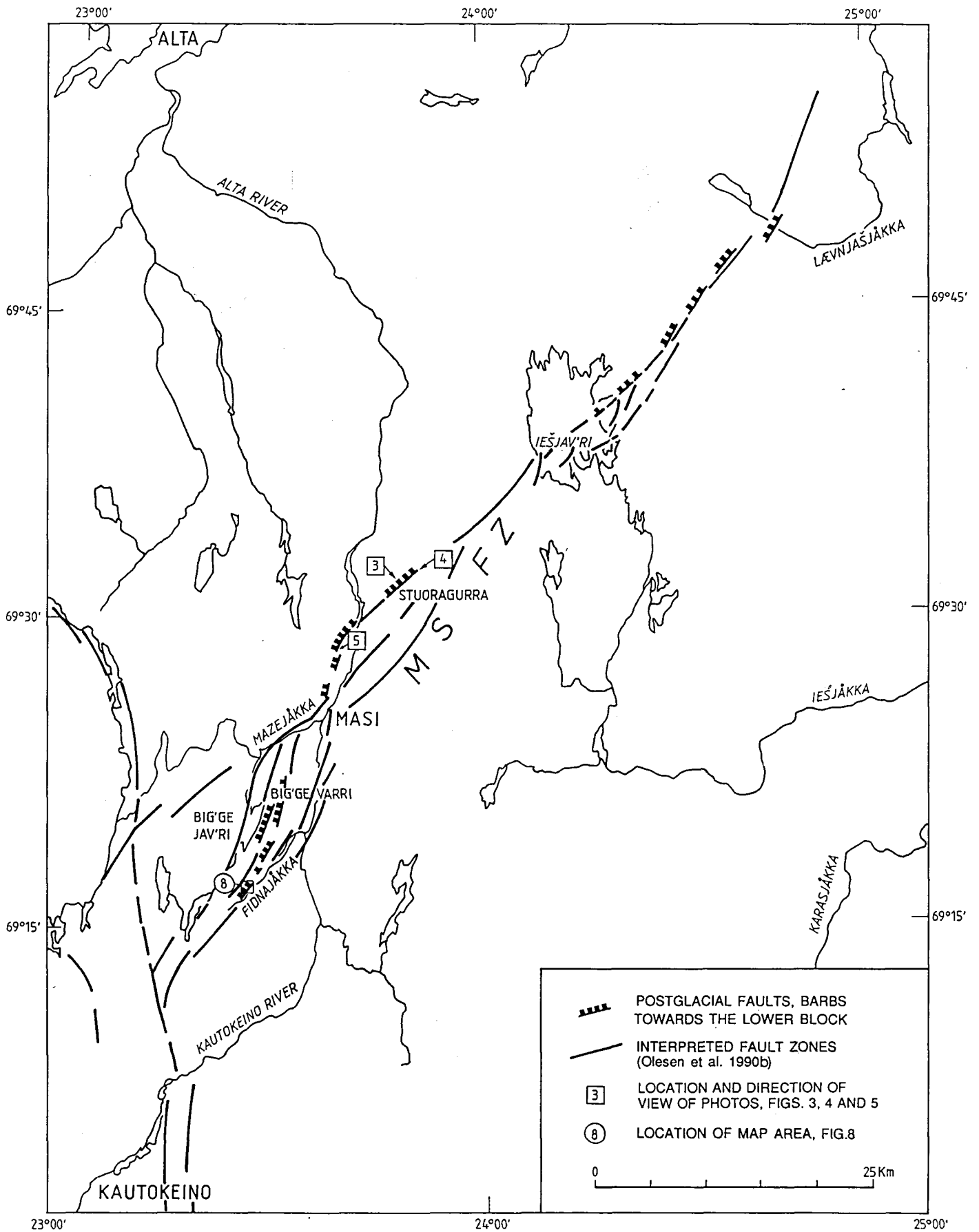


Fig. 2. Postglacial faults on Finnmarksvidda. MSFZ - Mierujav'ri-Sværholt Fault Zone.

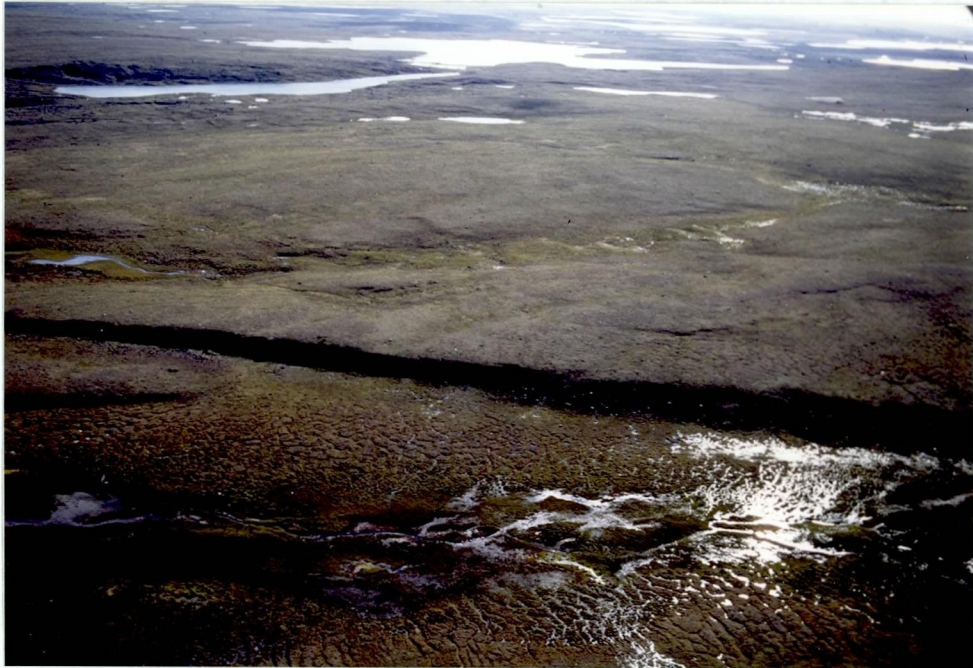


Fig. 3. Oblique aerial photograph of the Stuuragurra Fault (UTM 610200 - 7716200) looking east, approximately 10 km to the NNE of Masi. The location is shown in Fig. 2.



Fig. 4. The SF (in the middle of the picture) cutting through an esker 12 km NNE of Masi (UTM 611400 - 7717300); looking SW. The offset is approximately 2 m vertically and 0 - 5 m dextrally. The location is shown in Fig. 2.



Fig. 5. A 30 m long, 1 m wide and 1 m deep trench parallel to the escarpment in the hanging-wall block of the SF (UTM 604600 - 7710400). The distance from the slightly curved trench to the escarpment is 40 m. The location is shown in Fig. 2.

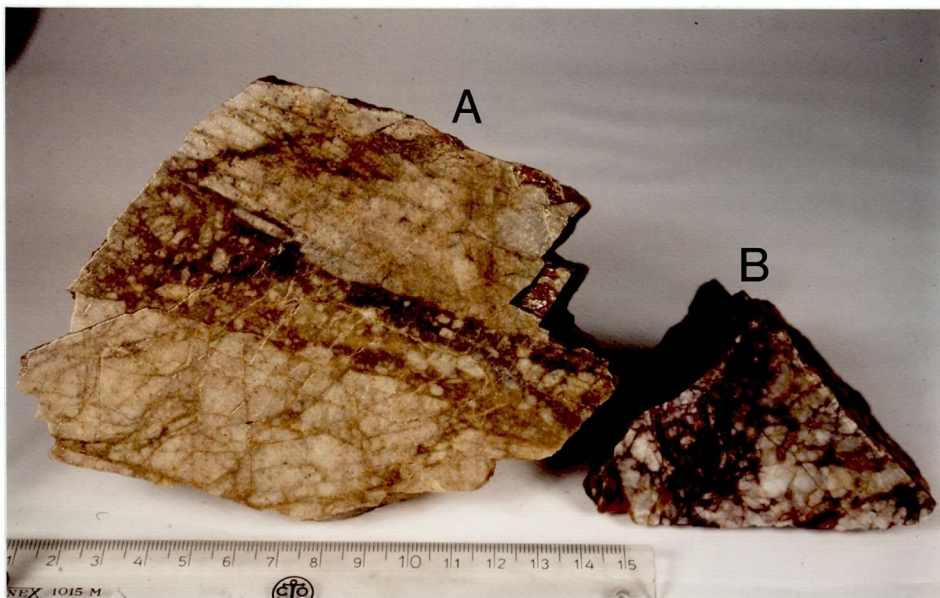


Fig. 6. Polished breccias of quartzite from the fault escarpment near Fidnajakka (UTM 596700 - 7687500). Mineral grains are crushed along fractures. The main secondary minerals present are chlorite (sample A) and ferrihydroxides (sample B). The sample location is the outcropping area shown in Fig. 16.

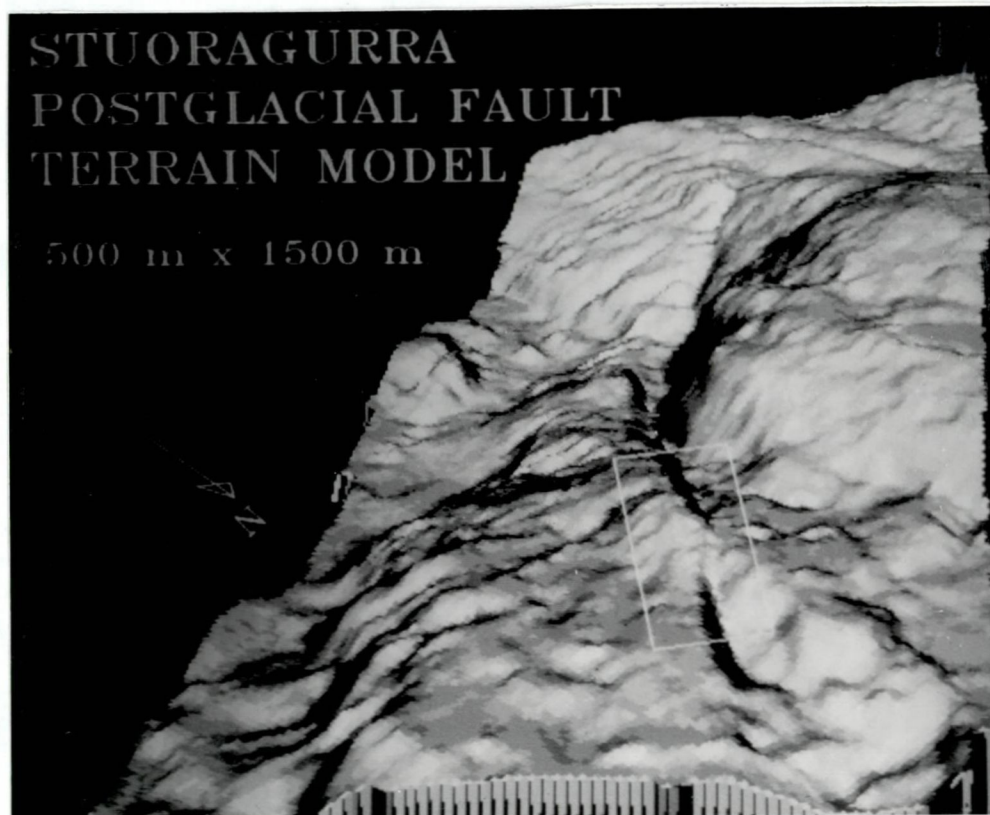


Fig. 7. 3D terrain model from the Fidnajäkka area. The vertical scale is exaggerated by a factor of 3. The survey area (Fig. 16) is indicated by the frame.

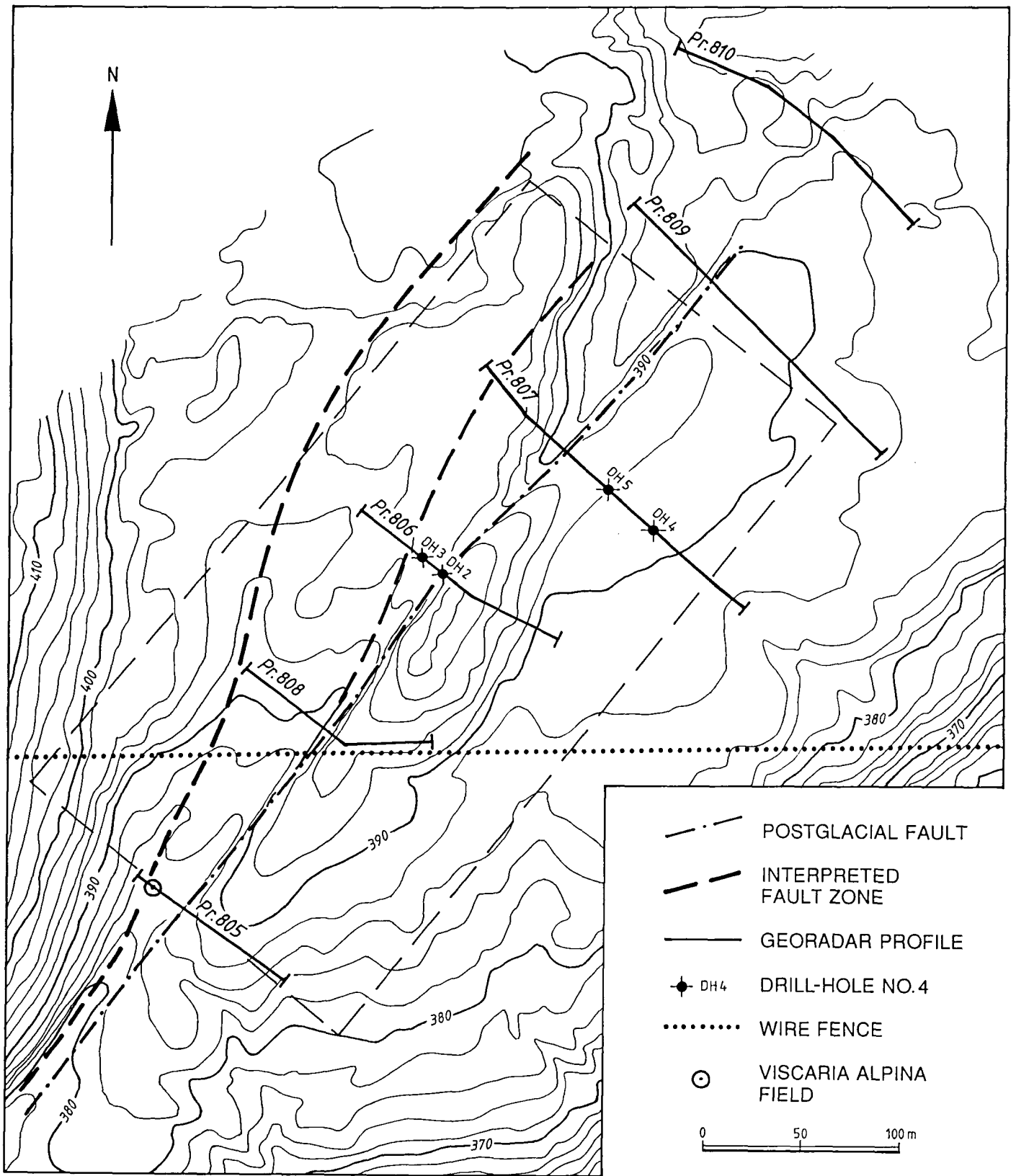
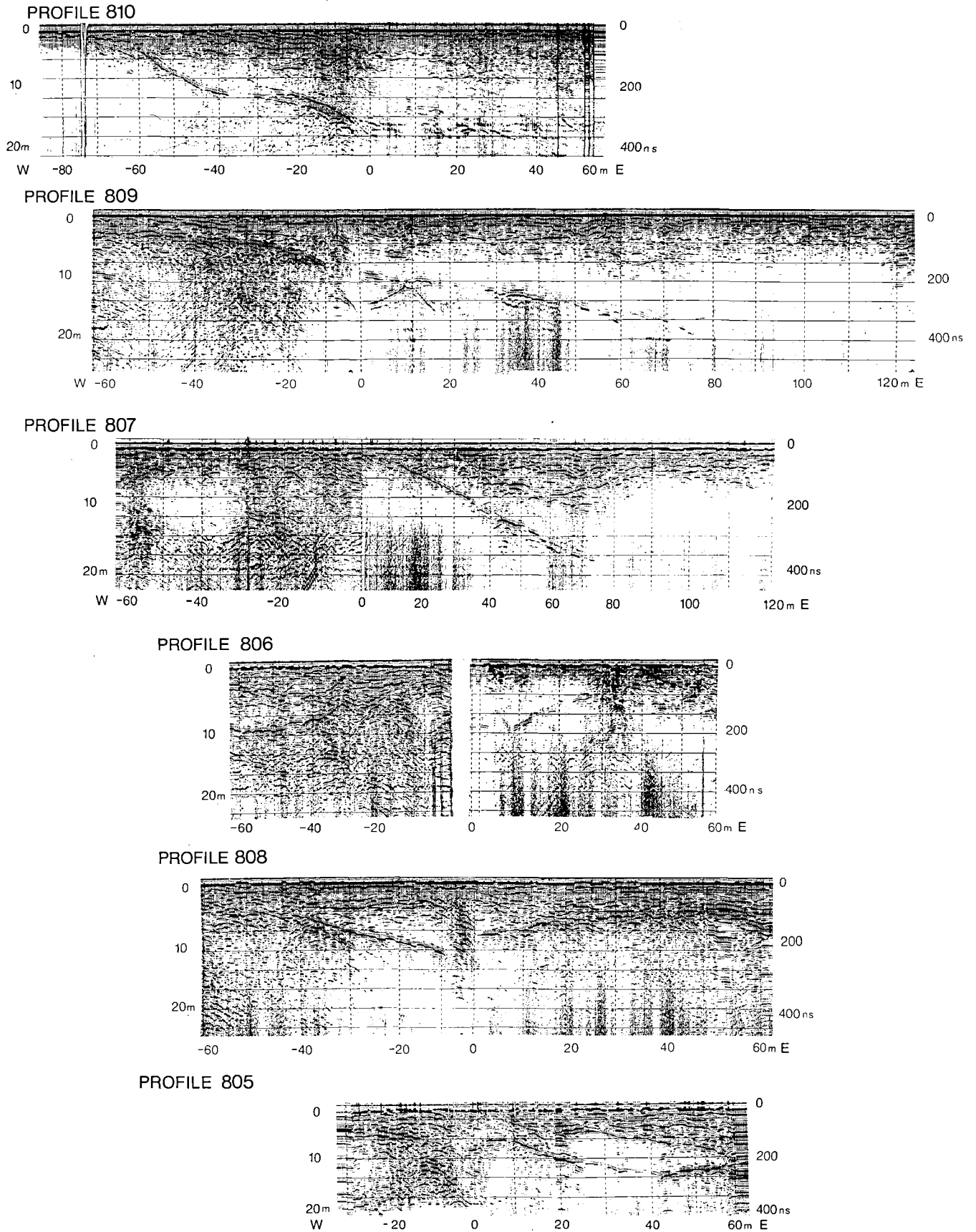


Fig. 8. Detailed topographical map from the Fidnajåkka area. The survey area (Fig. 16) is indicated by the frame.



GEORADAR, FIDNAJÄKKA



**Fig. 9. Georadar diagrams. Coordinate 0 on all the profiles is situated on the crest of the postglacial fault escarpment.**

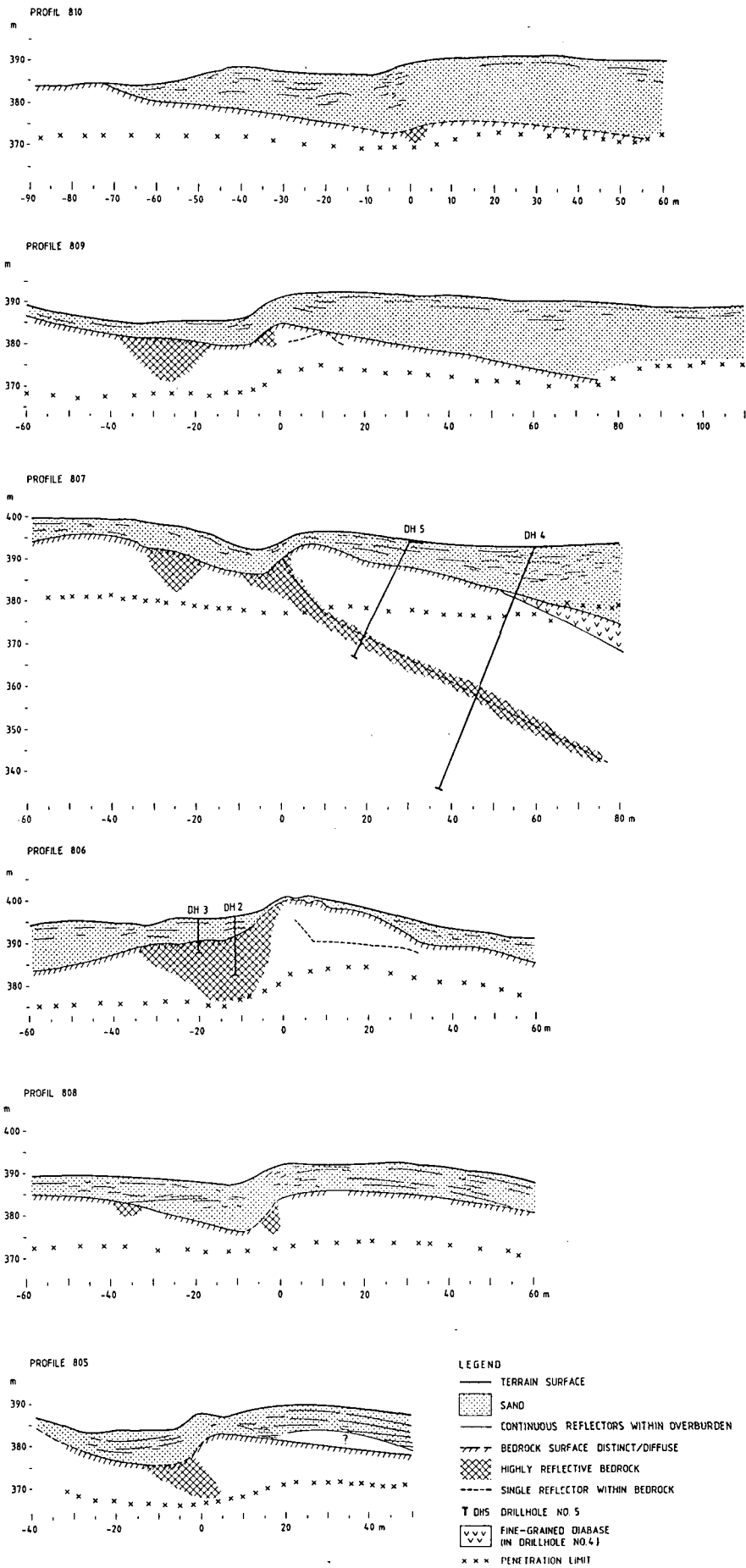


Fig. 10. Interpretation of georadar diagrams. Coordinate 0 on all the profiles is situated on the crest of the postglacial fault escarpment. In Profile 807, data from percussion drilling is added to the georadar interpretation below the penetration limit.

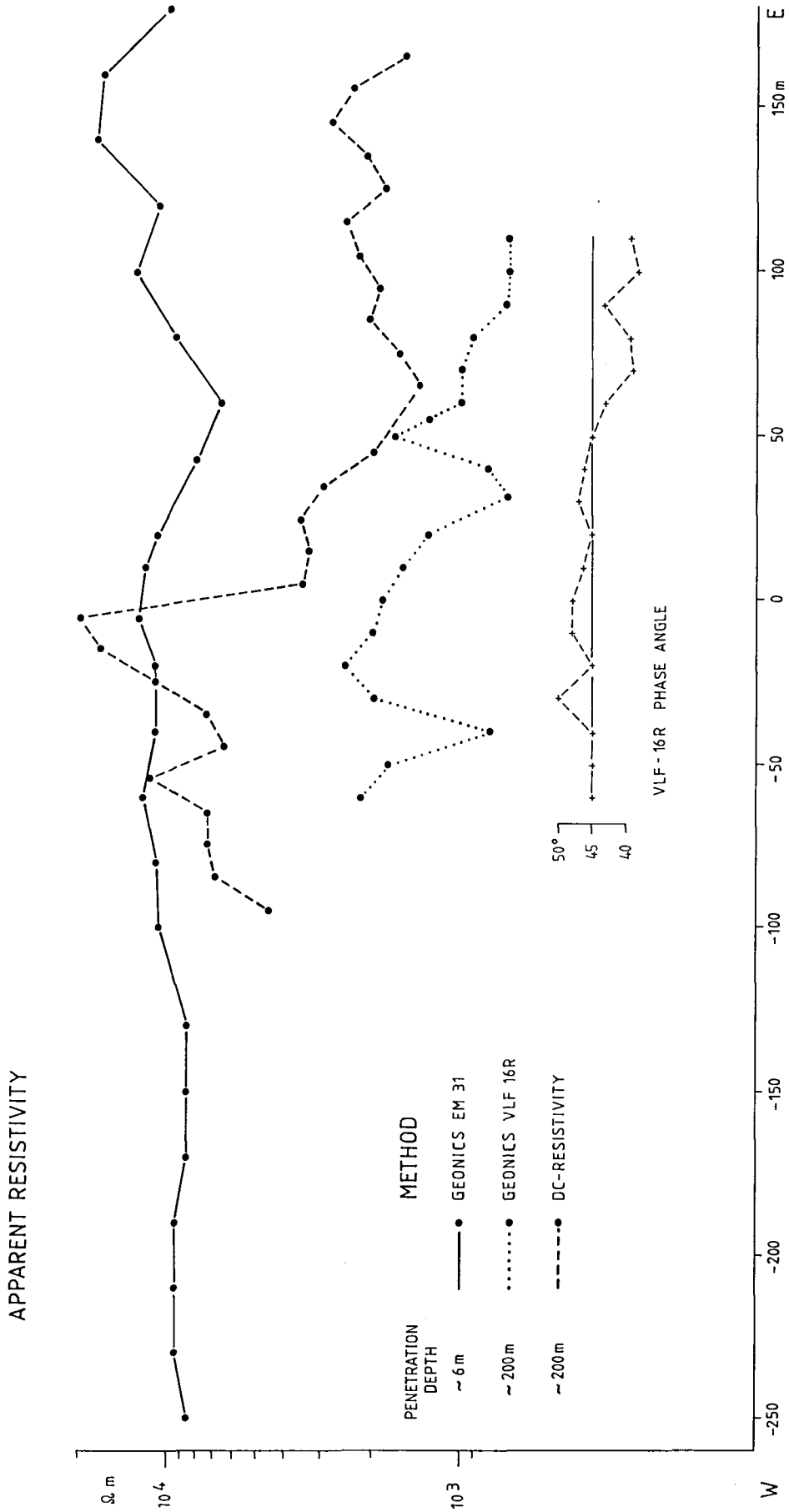


Fig. 11. Apparent resistivity measurements along Profile 807. The direction to the transmitter GYD (19 KHz) which is used for the VLF 16R measurements, is to the SW which is almost parallel to the postglacial fault

# SCHLUMBERGER VERTICAL ELECTRICAL SOUNDING FIDNAJÄKKA, PROFILE 807

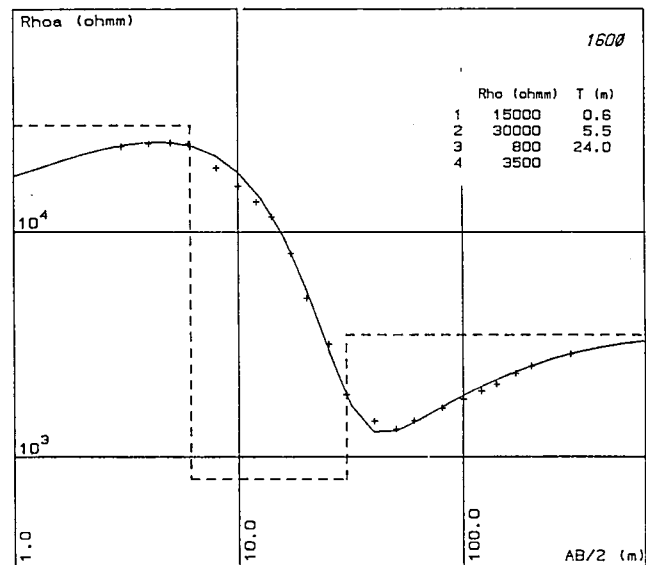
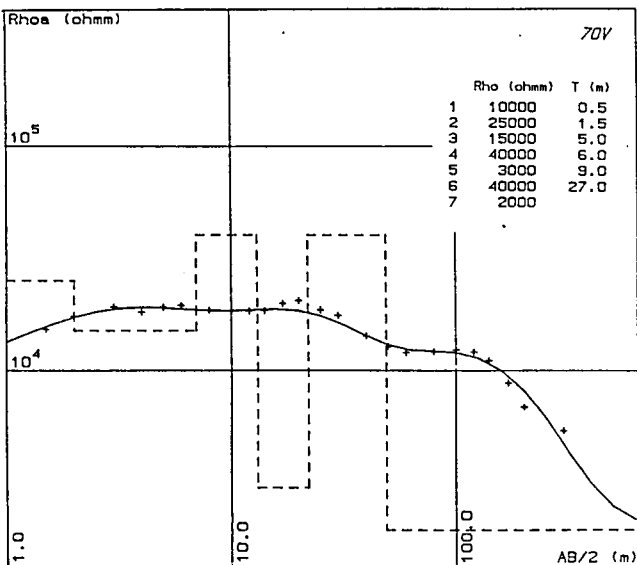
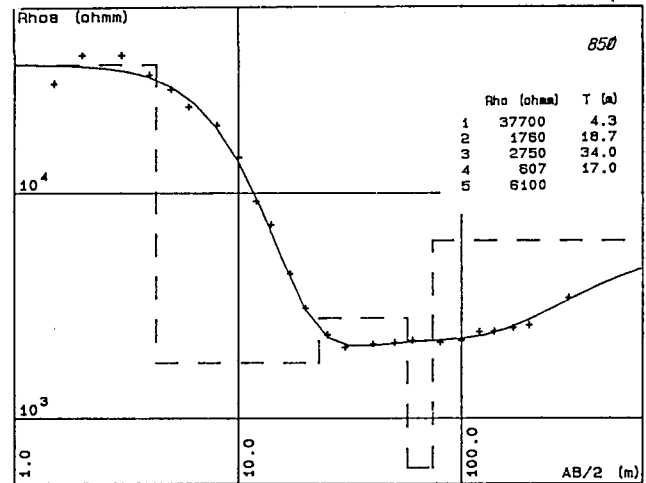
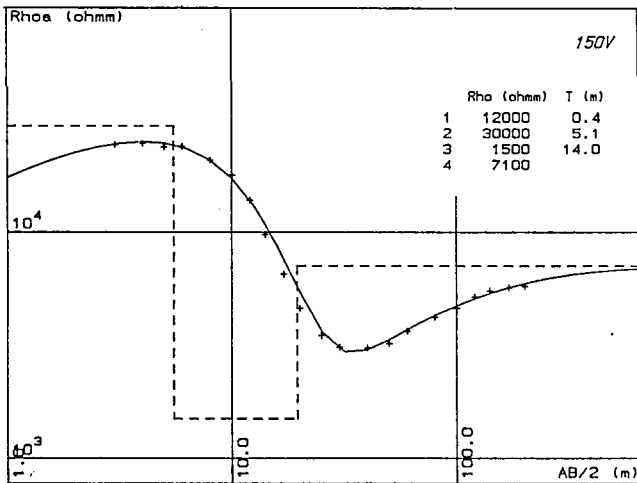
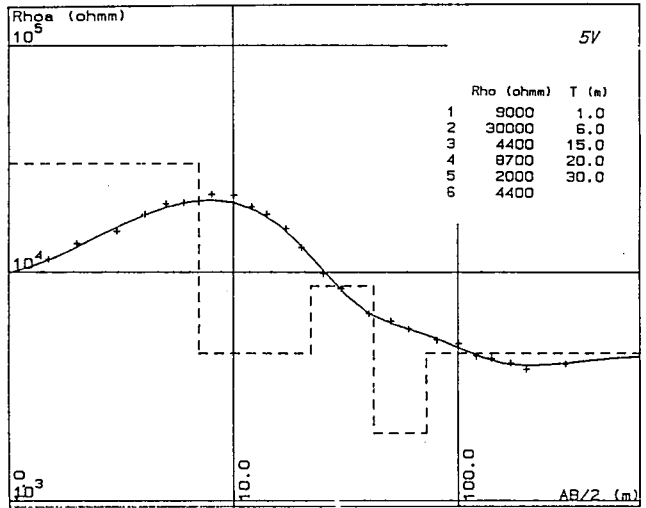
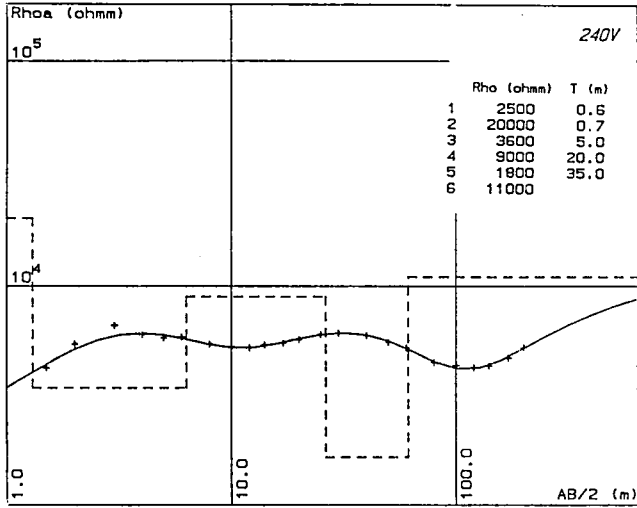


Fig. 12. Vertical electrical sounding along Profile 807.

VERTICAL ELECTRICAL SOUNDING  
PROFILE 807

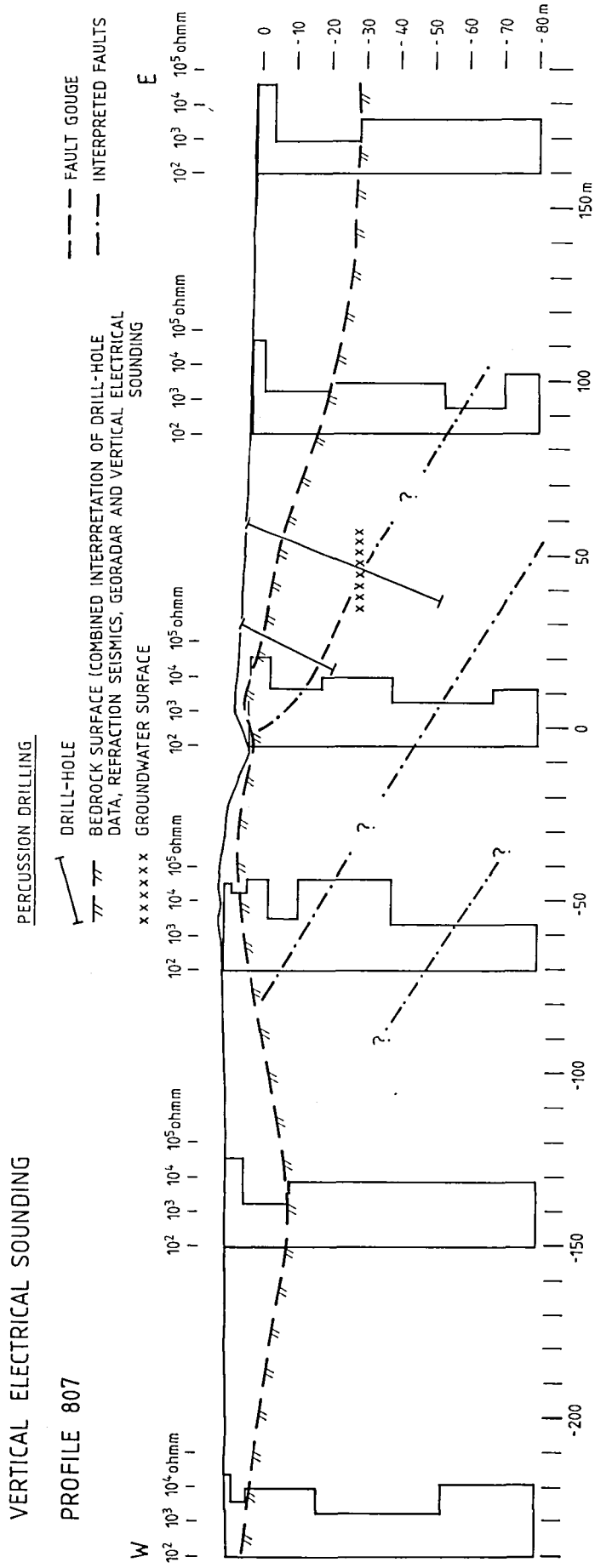
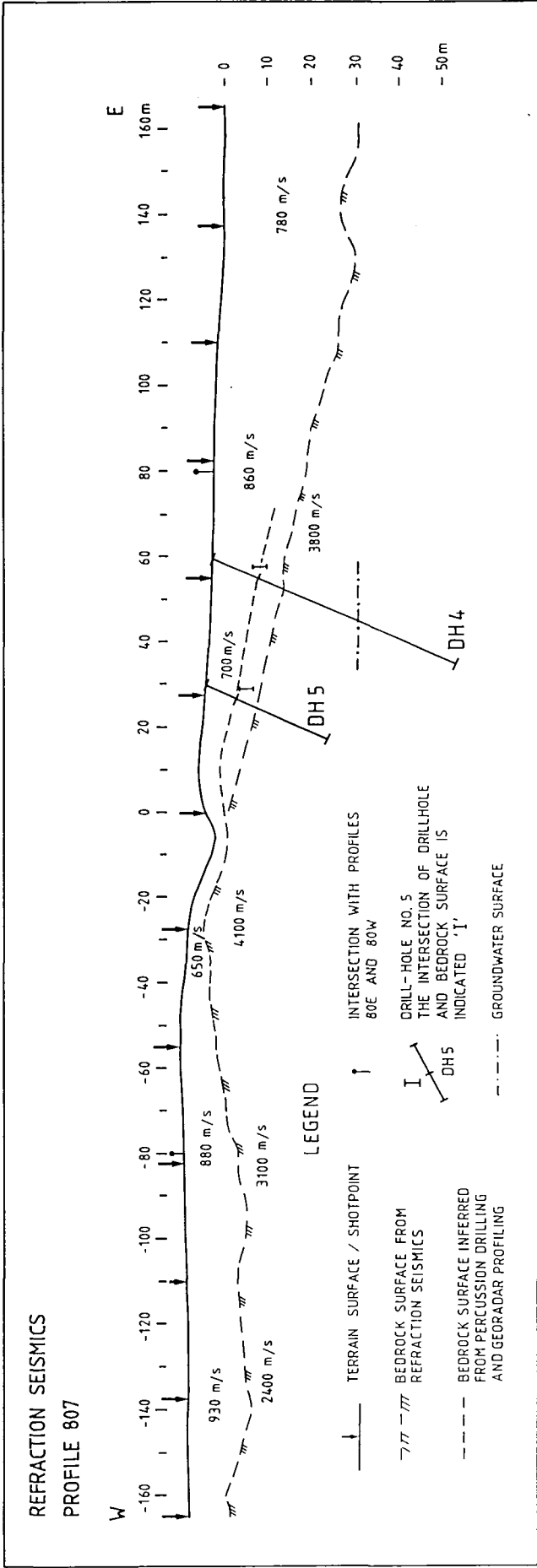


Fig. 13. Interpretation of vertical electrical sounding along Profile 807.

A



B

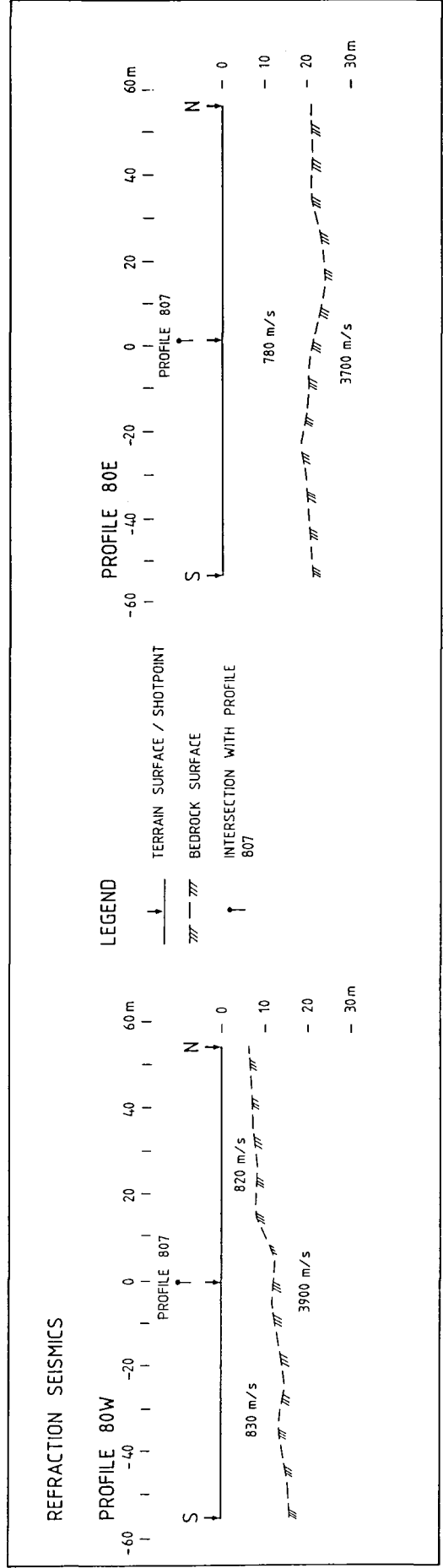
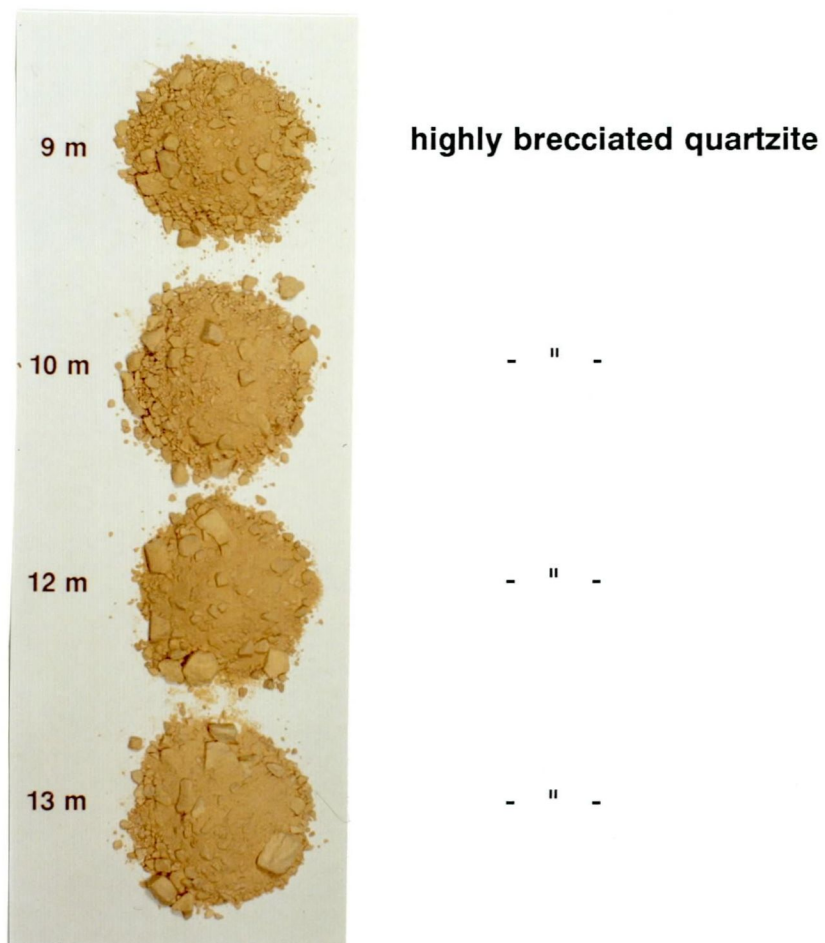


Fig. 14. A) Refraction seismics along Profile 807. B) Profiles intersecting Profile 807 at 80W and 80E, respectively.

**DRILLHOLE NO. 2**



**Fig. 15. Photograph of drill chips from the percussion drilling (continued over).**

**DRILLHOLE NO. 4**

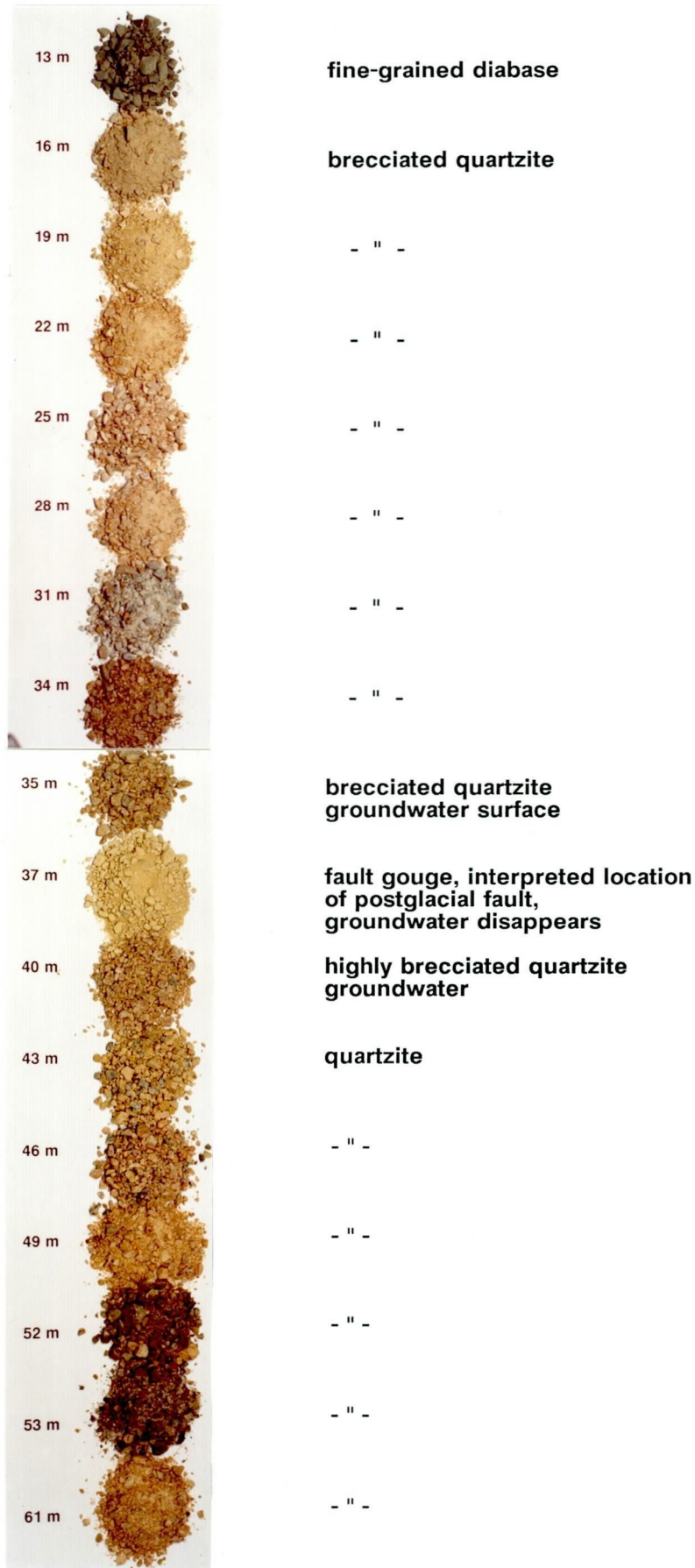


**Fig. 15. Continued**



**DRILLHOLE NO. 5**

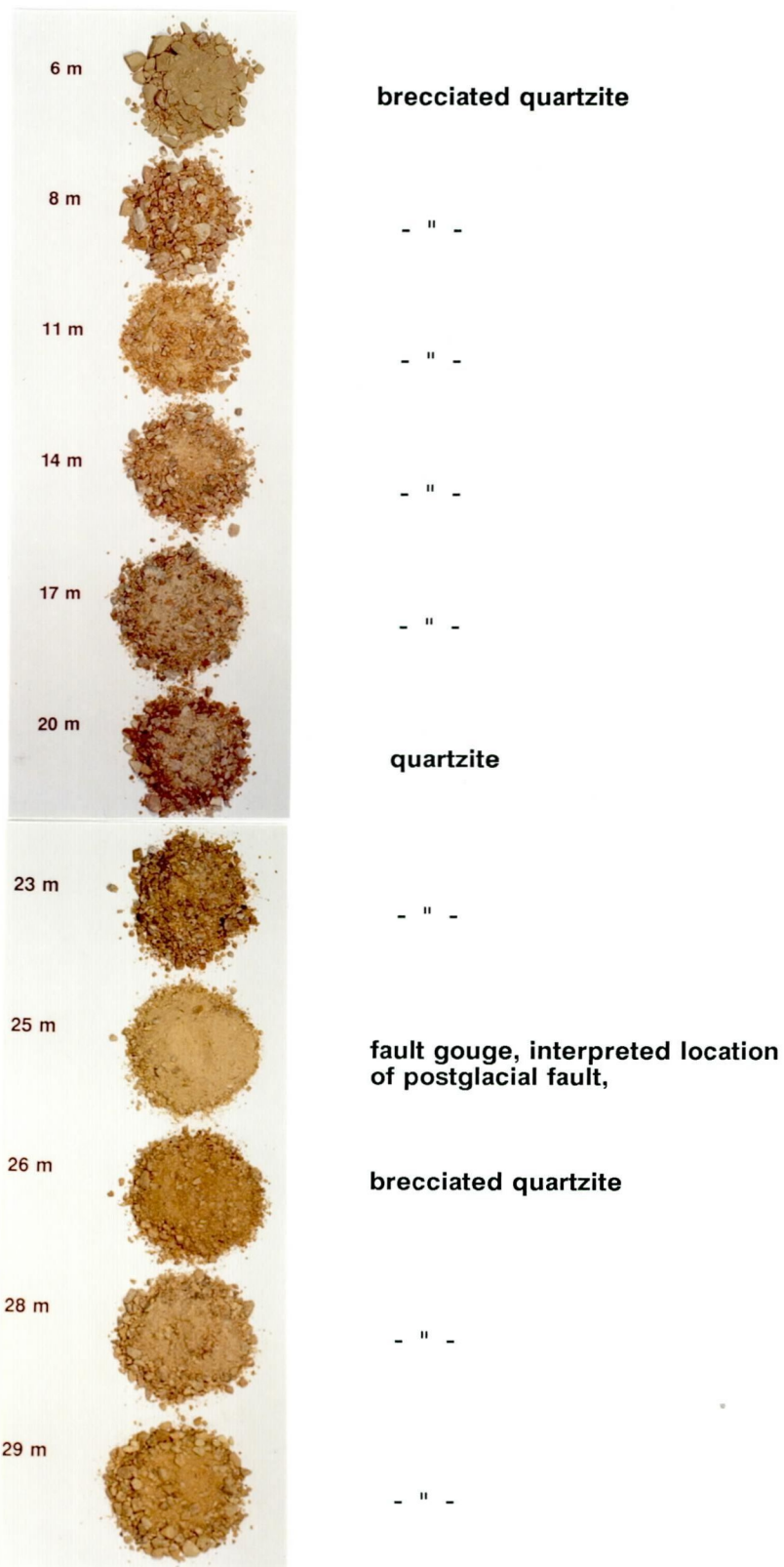


**Fig. 15. Continued**

# Stuoragurra postglacial fault

## Block diagram

### Fidnajåkka

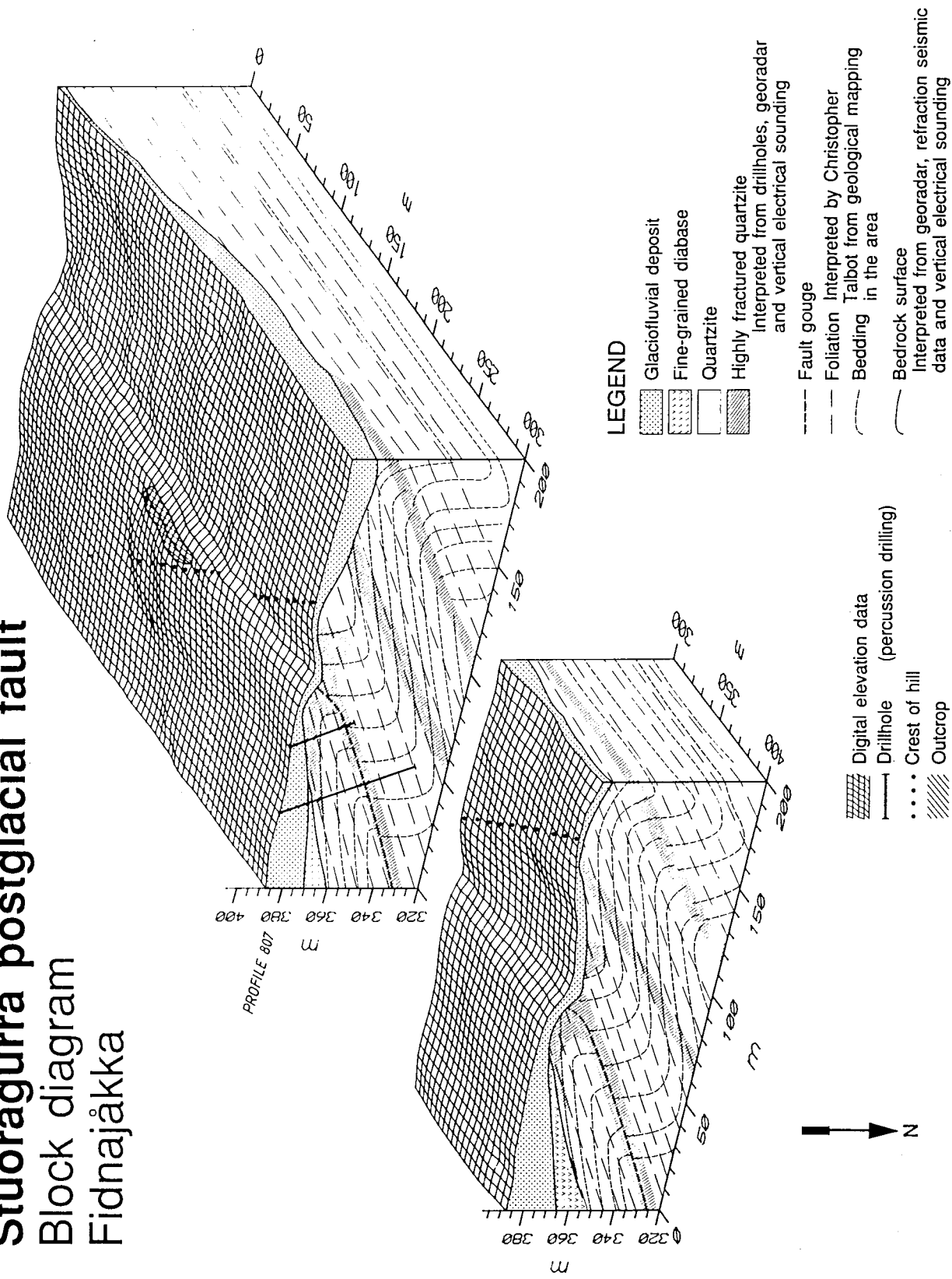


Fig. 16. Interpretation synthesis of model A (listric fault) for the SF as a block diagram, looking south. The location of the survey area is indicated by frames in Figs. 7 & 8. Note that Profile 807 in this diagram is a mirror image of the geophysical profiles along Profile 807 in Figs. 9-14 and that coordinate 85 in the present figure coincides with coordinate 0 in Figs. 9-14.